


Significant and Nonmonotonic Dynamic Magnetic Damping in Asymmetric Co-Fe/Ru/Co-Fe Trilayers

Yu Zhang, Guanjie Wu, Zhihao Ji, Xing Chen, Q. Y. Jin, and Zongzhi Zhang*

Shanghai Ultra-Precision Optical Manufacturing Engineering Research Center and Key Laboratory of Micro and Nano Photonic Structures (MOE), School of Information Science and Technology, Fudan University, Shanghai 200433, China

 (Received 13 September 2021; revised 3 January 2022; accepted 23 February 2022; published 11 March 2022)

Static and dynamic magnetic properties of Co-Fe(10 nm)/Ru($t_{\text{Ru}} = 0\text{--}3$ nm)/Co-Fe(5 nm) asymmetric trilayers are systematically investigated. The interlayer exchange coupling (IEC) strengths of bilinear (J_1), biquadratic (J_2), and their equivalent (J_{eff}) terms are determined; they show a weak nonmonotonic behavior with t_{Ru} . Interestingly, the magnetic remanence ratio η of hard axis to easy axis has two distinct peaks; this can reasonably be interpreted by taking the strong J_2 term into account. Various pump-laser fluences are utilized to modulate the static IEC during the time-resolved magneto-optical Kerr effect measurements, by which individual magnetization precessions of the two Co-Fe layers are achieved and the effects of dynamic IEC through mutual spin currents are highlighted. With the increase in t_{Ru} , the magnetic damping factors of both layers display the same nonmonotonic behavior, which has been mainly ascribed to the spin pumping damping α_{SP} associated with the dynamic IEC. Moreover, it is found that the variation trend of damping difference $\Delta\alpha_{\text{SP}}$ between the two Co-Fe layers is similar to that of J_{eff} , revealing that the dynamic IEC effect is actually dominated by the static IEC and thereupon a theoretical formula is proposed to describe the correlation between $\Delta\alpha_{\text{SP}}$ and J_{eff} . These results suggest the feasibility of efficient control of spin pumping damping through controlled IEC, which has great significance for microwave spintronic devices based on asymmetric trilayer structures.

DOI: [10.1103/PhysRevApplied.17.034033](https://doi.org/10.1103/PhysRevApplied.17.034033)

I. INTRODUCTION

After the discovery of the giant magnetoresistance effect in the synthetic antiferromagnetic (SAF) structure of Fe/Cr/Fe [1,2], magnetic trilayer films, in which the two ferromagnetic (FM) layers are ferromagnetically coupled or antiferromagnetically (AFM) coupled through a nonmagnetic (NM) spacer, have been extensively investigated and applied as the pinned layer of spin valves or magnetic tunnel junctions in modern magnetic memories or logic devices [3–6]. In recent years, SAF structures have attracted a greatly renewed interest in line with the emerging field of antiferromagnetic spintronics [7], including tunnel magnetoresistance devices [8], magnetic racetrack memories [9, 10], three-dimensional logic units [11], robust field-free spin-orbit-torque switching elements [12–14], and especially high frequency applications. Because of the ultrahigh frequency of the optical resonance mode [15–18], the asymmetric FM/NM/FM sandwiched structure with strong interlayer exchange coupling (IEC) has been considered as a potential solution to breaking through the frequency limitation of micromagnetic inductors, filters,

phase shifters, and monolithic microwave integration circuits [19–21]. All these applications require deep insights into the physical nature of the synthetic trilayers. Apart from the magnetic precession mode and precession frequency [22–24], much attention should also be paid to the magnetic damping factor, since it describes not only the energy dissipation rate of magnetization precession, but also the magnitude of required driving source (e.g., charge current or spin current). For the coupled trilayer SAF structure, besides the well-known oscillatory IEC mediated via the conduction electrons and described by the Ruderman-Kittel-Kasuya-Yosida (RKKY) theory [25], an observable dynamic interlayer coupling mediated by the pumped spin current would also be expected [26–28]. In order to accelerate the advanced applications of these asymmetric SAF systems with ultrafast magnetization manipulation and low energy consumption, the nonlocal spin pumping damping induced by dynamic IEC during persistent oscillation procedures deserves to be systematically explored.

As is known to all, precessing magnetizations are capable of transferring spin angular momentum into an adjacent NM layer. If the FM/NM bilayer has a large interfacial spin-mixing conductance and the NM layer thickness is much greater than the spin diffusion length, the pumped spin current will diffuse across the FM/NM interface and

*zzzhang@fudan.edu.cn

dissipate completely within the NM layer, leading to a rather high spin pumping damping contribution [29,30]. Otherwise, the spin current will be reflected back to the FM layer, showing a negligible impact on the magnetization dynamics. However, for the trilayer system of $\text{FM}_1/\text{NM}/\text{FM}_2$ with a thin NM layer, the spin current generated by magnetization precession of FM_1 (or FM_2) will pass through the NM spacer and enter the other FM_2 (or FM_1) layer, thereby making the two FM layers feel each other through the spacer by exchanging nonequilibrium spin currents. Such a dynamic coupling between the two precessing magnetizations can also result in a “spin-momentum brake” and further enhance the magnetic damping of the two FM layers with different resonance frequencies [27]. It has been shown that in addition to the normal coherent precession (acoustic mode), an out-of-phase precession mode (optic mode) can also be detected for the trilayer samples [22,31]. The optical mode always has a larger magnetic damping than the acoustic mode, because the spin current and spin accumulation are greatly enhanced for the out-of-phase precession [22,32,33]. Lenz *et al.* observed an oscillatory damping behavior for both the acoustic and optic modes with increasing Cu interlayer thickness, illustrating that the dynamic and static parts of the IEC contribute to the large nonlocal spin pumping damping [34]. Nevertheless, Belmeguenai *et al.* showed a clearly different behavior of the ferromagnetic resonance linewidths for the two modes in the coupled Ni-Fe/Ru/Ni-Fe thin films; i.e., the damping of the acoustic mode is almost constant while that of the optic mode oscillates as a function of the Ru layer thickness [35]. These results are distinctly different, suggesting that the detailed effect of IEC on the overall damping of trilayer structures and the profound relations between the dynamic and static IEC are still unclear, which limits the performance improvement of spintronic devices.

Apparently, the magnetic dynamic behaviors rely not only on the static RKKY coupling, but also on the dynamic IEC. In order to achieve fast manipulation of magnetization orientation and low energy consumption, more elaborate investigations should be performed to acquire convincing experimental results and fully clarify the underlying mechanism. Time-resolved magneto-optical Kerr effect (TRMOKE) spectroscopy is an excellent tool for investigating dynamic magnetic properties in the time domain, which can simultaneously excite magnetization precessions in the two magnetic layers, allowing us to explore the influences of static and dynamic IEC on the respective precessional behaviors of the coupled trilayer system. In this work, we report a comprehensive study on the static and dynamic magnetic properties of asymmetric Co-Fe(10 nm)/Ru(0–2.9 nm)/Co-Fe(5 nm) films. Considering that the Ru spacer has a long spin diffusion length of $\lambda_{\text{SD}} \sim 10$ nm [36], the dynamic interlayer coupling via spin current would exist during the laser-induced

magnetization precession dynamics [26,27]. To highlight the role of dynamic IEC on the magnetization behaviors, various pump-laser fluences are employed to modulate the static IEC strength. An obvious nonmonotonic behavior is found for the extracted damping factors of the two FM layers, which can be attributed to the mutual spin pumping current based on the dynamic IEC. Further analyses illustrate a similar variation tendency between the difference of spin pumping damping and the effective static coupling strength, which suggest the feasibility of efficient control of magnetic damping through controlled IEC.

II. EXPERIMENTAL SECTION

Samples with a structure of $\text{Co}_{80}\text{Fe}_{20}(10 \text{ nm})/\text{Ru}(t_{\text{Ru}} = 0\text{--}2.9 \text{ nm})/\text{Co}_{80}\text{Fe}_{20}(5 \text{ nm})/\text{Al}(5 \text{ nm})$ are fabricated by dc magnetron sputtering under a base pressure better than 3.0×10^{-8} torr. Before film deposition, the single-crystalline MgO(001) substrates are preheated at 600°C for 30 min to get a clean surface. The bottom 10-nm-Co-Fe layer is found to be epitaxially grown while the top 5-nm-Co-Fe layer is proved to be disordered due to the insertion of the Ru spacer. The magnetic hysteresis loops and angular remanence magnetization (ARM) curves are measured by a vibrating sample magnetometer (VSM). The magnetization dynamics are investigated by a femtosecond laser pump-probe system with a central wavelength of 800 nm, a pulse duration of 150 fs, and a repetition rate of 1000 Hz [37]. The dynamic behaviors are excited by an intense pump pulse beam, and the transient MOKE signals are detected by a time-delayed weak probe beam in a polar geometry. The TRMOKE signals are read out by a lock-in amplifier with an optical chopper, which modulates the pump beam at a frequency of 108 Hz. During the TRMOKE measurements, various pump-laser beam fluences in the range of 1.3–12.8 mJ/cm^2 are employed to control the transient static IEC strength. A variable external magnetic field with a maximum of 12.3 kOe is applied at a field angle of 71° from the film normal. Note that all the measurements are conducted at room temperature in this work.

III. RESULTS AND DISCUSSION

A. Static magnetic measurements by VSM

In order to help interpret the static magnetic properties and the subsequent TRMOKE results quantitatively, a polar coordinate system is established. As sketched in Fig. 1(a), M_1 , t_1 and M_2 , t_2 represent the magnetizations and thicknesses of the 10-nm Co-Fe (denoted as FM_1) and 5-nm Co-Fe (FM_2), respectively. The azimuthal angle and polar angle of magnetization \mathbf{M} (applied field \mathbf{H}) are defined as φ_M (φ_H) and θ_M (θ_H). Figure 1(b) displays the in-plane M - H loops of MgO(001)/Co-Fe(10 nm) with $\varphi_H = 0^\circ$ and 45° , and the inset shows the corresponding

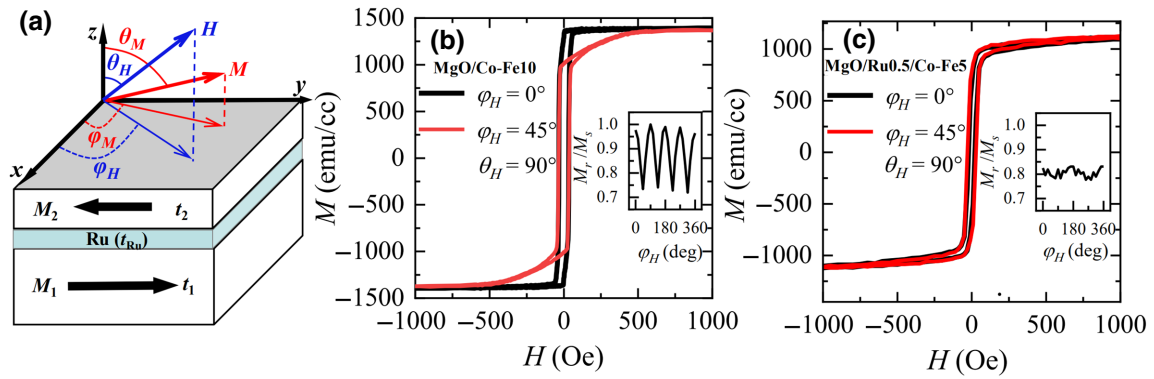


FIG. 1. (a) The polar coordinate system established for the analyses of magnetic measurement results. (b) The in-plane ($\theta_H = 90^\circ$) M - H loops of MgO(001)/Co-Fe(10 nm) for $\varphi_H = 0^\circ$ (easy axis) and 45° (hard axis). (c) The in-plane M - H loops of MgO(001)/Ru(0.5 nm)/Co-Fe(5 nm) for $\varphi_H = 0^\circ$ and 45° , showing negligible magnetic anisotropy. The insets in (b) and (c) denote the corresponding magnetic remanence ratios as a function of φ_H .

curve of ARM. The saturation magnetization M_s is calculated to be 1380 emu/cm^3 . Clearly, the Co-Fe film shows a definite biaxial anisotropy with easy axis along $\varphi_H = 0^\circ$ and hard axis along $\varphi_H = 45^\circ$, suggesting that the FM₁ layer of Co-Fe(10 nm) is epitaxially grown and has a cubic structure. The in-plane anisotropy field can be numerically determined to be approximately 700 Oe via fitting the hard axis magnetization curves. Figure 1(c) depicts the in-plane M - H loops of MgO(001)/Ru(0.5 nm)/Co-Fe(5 nm). The M_s value here is only 1112 emu/cm^3 , which can be attributed to the relatively large contribution of interfacial magnetic dead layer for the thin Co-Fe layer as well as the disordered crystalline structure. As shown in the inset, in contrast to the epitaxially grown 10-nm Co-Fe with a four-fold anisotropy, the 5-nm-Co-Fe layer on top of the Ru has a negligible twofold anisotropy, demonstrating that the top FM₂ layer is almost isotropic.

Figure 2(a) shows the representative in-plane M - H loops of MgO(001)/Co-Fe(10 nm)/Ru(t_{Ru})/Co-Fe(5 nm) trilayers with the applied field along either the easy or hard axis. The two FM layers are ferromagnetically coupled for $t_{\text{Ru}} < 0.4 \text{ nm}$; after that they become AFM coupled. As t_{Ru} is further increased to more than 2.0 nm, the two Co-Fe layers get decoupled due to the negligible IEC. A typical AFM coupled M - H loop can be seen for the case of $t_{\text{Ru}} = 1.1 \text{ nm}$, showing an obvious plateau at the region close to zero field, which indicates the antiparallel magnetization alignment between the two Co-Fe layers. Interestingly, although the sample of $t_{\text{Ru}} = 0.5 \text{ nm}$ also has strong AFM coupling with a saturation field as high as about 8.0 kOe (see the inset), no obvious plateau can be observed. This can be ascribed to the larger biquadratic coupling term of J_2 , which gives rise to the formation of a spin-flop phase at the remanence state. In order to explore the mechanism of the t_{Ru} dependence of the spin-flop phase, here we define the remanence ratio of hard axis ($\varphi_H = 45^\circ$) to easy axis ($\varphi_H = 0^\circ$) as η . Figure 2(b)

denotes the value of η as a function of t_{Ru} . For $t_{\text{Ru}} = 0 \text{ nm}$, the two FM layers are directly coupled and behave as a single layer. Obvious magnetic anisotropy can be observed and the remanence ratio is extracted to be 0.71, as displayed in Fig. 2(b), which is consistent with the ideal value for a perfect biaxially anisotropic structure. As for the trilayer samples with an intermediate t_{Ru} of 0.4–2.0 nm, the two FM layers are AFM coupled via the indirect RKKY interaction. Assuming the magnetization orientation of Co-Fe(5 nm) is strictly antiparallel to that of Co-Fe(10 nm), their net magnetization can be roughly regarded as a 5-nm-thick Co-Fe with the same biaxial magnetic anisotropy as FM₁, which will give rise to a constant η value close to 0.71, as indicated by the blue dashed line in Fig. 2(b). However, a nonmonotonic variation trend is observed, with two distinct peaks occurring at $t_{\text{Ru}} = 0.5 \text{ nm}$ and 1.4 nm. This suggests that in addition to the RKKY-type bilinear coupling (J_1), which tends to drive the magnetizations to be aligned parallel or antiparallel, there also exists a non-negligible 90° biquadratic coupling term (J_2). Generally, the biquadratic coupling is much smaller than the bilinear one [2,22], whereas in some IEC systems with fourfold anisotropy a large J_2 may emerge that could even dominate the static and dynamic properties [38–40]. It is worth noting that when J_2 is comparable to J_1 , a spin-flop phase would always be formed, resulting in an increase in remanence ratio [35]. Therefore, we consider that the observed complicated behavior of η arises from the competition among the bilinear coupling, biquadratic coupling, and magnetic biaxial anisotropy, which determines the equilibrium position of magnetization in the absence of an external field. When t_{Ru} is raised to more than 2.0 nm, where the IEC disappears, an increase in η to approximately 0.77 is found, which can be attributed to the simple superposition of the biaxial anisotropic Co-Fe(10 nm) and the isotropic Co-Fe(5 nm) layers. Considering that the ideal η value is $\cos 45^\circ \sim 0.71$ for films

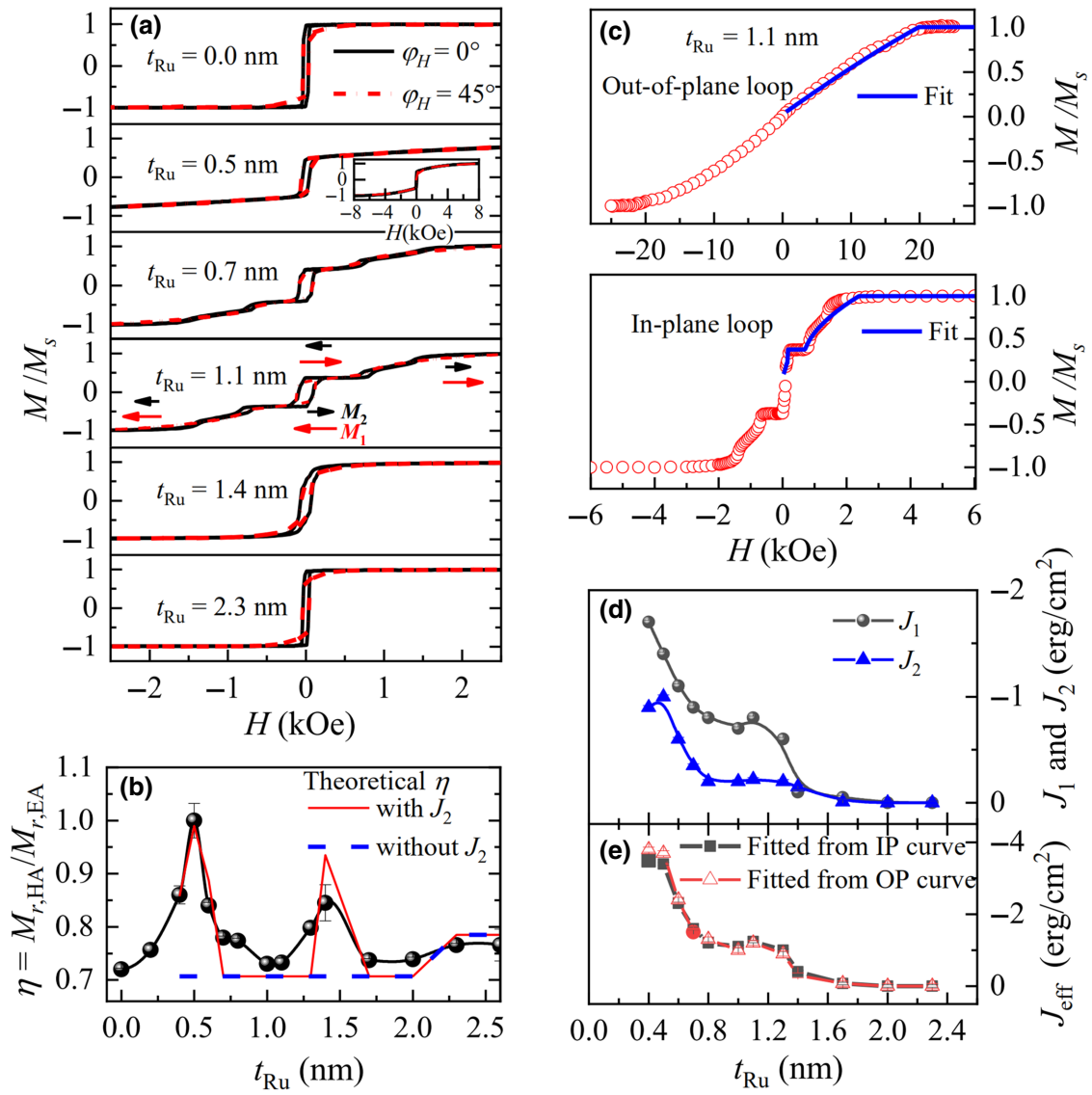


FIG. 2. (a) The in-plane M - H loops of Co-Fe(10 nm)/Ru(t_{Ru})/Co-Fe(5 nm) trilayers with various t_{Ru} for $\varphi_H = 0^\circ$ and 45° ; the inset depicts the M - H loop of $t_{\text{Ru}} = 0.5$ nm in the field range of ± 8.0 kOe. (b) The remanence ratio η of hard axis (HA) to easy axis (EA) as a function of t_{Ru} and the corresponding theoretical values with J_2 or without J_2 . (c) The out-of-plane and in-plane magnetic hysteresis loops with $t_{\text{Ru}} = 1.1$ nm and $\varphi_H = 0^\circ$. The blue solid lines are the corresponding fittings. (d) The t_{Ru} dependences of fitted J_1 and J_2 values from the in-plane loops, and (e) J_{eff} values obtained by fitting the in-plane (IP) and out-of-plane (OP) loops.

with biaxial anisotropy and $\cos 0^\circ = 1$ for isotropic ones, the overall η of the decoupled trilayer can be theoretically calculated to be about 0.78, according to the relation of $\eta = (0.707M_{s,1}t_1 + M_{s,2}t_2)/(M_{s,1}t_1 + M_{s,2}t_2)$.

To gain quantitative insights into the underlying mechanism of the abnormal variation trend for η , the exchange coupling constants of J_1 and J_2 should be extracted. The IEC energy density E_{ex} can be expressed phenomenologically as

$$E_{\text{ex}} = -J_1 \frac{\mathbf{M}_1 \cdot \mathbf{M}_2}{M_1 M_2} - J_2 \left(\frac{\mathbf{M}_1 \cdot \mathbf{M}_2}{M_1 M_2} \right)^2, \quad (1)$$

where \mathbf{M}_1 and \mathbf{M}_2 are the magnetization vectors of the two FM layers, and J_1 and J_2 are the bilinear and biquadratic coupling parameters, respectively. When J_1 dominates, \mathbf{M}_1 and \mathbf{M}_2 prefer to stay parallel for $J_1 > 0$ or antiparallel for $J_1 < 0$. However, if J_2 dominates and $J_2 < 0$, \mathbf{M}_1 and \mathbf{M}_2 favor a 90° alignment. In this study, for our continuous trilayer films with in-plane magnetic anisotropy, only the uniform magnetization precessions are excited in our TRMOKE experiments, so that both the self- and mutual-dipolar fields associated to the nonuniform precession ($k \neq 0$, where k is the spin wave number) of the two FMs are ignored [41]. Therefore, the areal density of free energy E includes the Zeeman energy, magnetic anisotropy

energy, demagnetization energy, and interlayer coupling energy [42],

$$\begin{aligned}
E = E_{\text{Zeeman}} + E_{\text{anis}} + E_{\text{dem}} + E_{\text{ex}} = & \sum_{i=1,2} t_i \{-M_{s,i} H [\sin \theta_{M,i} \sin \theta_H \cos(\varphi_{M,i} - \varphi_H) + \cos \theta_{M,i} \cos \theta_H] \\
& - \frac{1}{8} (3 + \cos 4\varphi_{M,i}) K_{B,i} \sin^4 \theta_{M,i} + K_{\perp,i} \sin^2 \theta_{M,i} - 2\pi M_{s,i}^2 \sin^2 \theta_{M,i}\} \\
& - J_1 [\sin \theta_{M,1} \sin \theta_{M,2} \cos(\varphi_{M,1} - \varphi_{M,2}) + \cos \theta_{M,1} \cos \theta_{M,2}] \\
& - J_2 [\sin \theta_{M,1} \sin \theta_{M,2} \cos(\varphi_{M,1} - \varphi_{M,2}) + \cos \theta_{M,1} \cos \theta_{M,2}]^2, \quad (2)
\end{aligned}$$

where $t_{1(2)}$, $M_{s,1(2)}$, $K_{B,1(2)}$ and $K_{\perp,1(2)}$ are the thickness, saturation magnetization, and in-plane biaxial and out-of-plane uniaxial magnetic anisotropy constant of FM₁ (and FM₂), respectively. We define $H_{B,i} = 4K_{B,i}/M_{s,i}$ as the in-plane biaxial anisotropy field and $H_{K,i} = 2K_{\perp,i}/M_{s,i}$. Considering the isotropic nature of FM₂, we neglect the $K_{B,2}$ term in the following analyses for simplicity. According to the Stoner-Wohlfarth coherent rotation model [43], the equilibrium position equations of \mathbf{M}_1 and \mathbf{M}_2 can be determined from the minimum of free energy density E . When H is applied within the film plane ($\theta_H = 90^\circ$), the equilibrium equations are

$$\begin{aligned}
H \sin(\varphi_H - \varphi_{M,1}) = & \frac{1}{8} H_{B,1} \sin 4\varphi_{M,1} \\
& + \frac{J_1 \sin \Delta\varphi + J_2 \sin 2\Delta\varphi}{t_1 M_{s,1}} \\
H \sin(\varphi_{M,2} - \varphi_H) = & \frac{J_1 \sin \Delta\varphi + J_2 \sin 2\Delta\varphi}{t_2 M_{s,2}}. \quad (3)
\end{aligned}$$

When H is along the film normal ($\theta_H = 0^\circ$) with $\varphi_{M,1} = 0^\circ$ and $\varphi_{M,2} = 180^\circ$ (J_1 dominated), we have

$$\begin{aligned}
2H \sin \theta_{M,1} = & \frac{1}{2} H_{B,1} \sin^2 \theta_{M,1} \sin 2\theta_{M,1} - H_{\text{keff},1} \sin 2\theta_{M,1} \\
& - \frac{2 \sin \theta}{t_1 M_{s,1}} (J_1 + 2J_2 \cos \theta) \\
2H \sin \theta_{M,2} = & -H_{\text{keff},2} \sin 2\theta_{M,2} - \frac{2 \sin \theta}{t_2 M_{s,2}} (J_1 + 2J_2 \cos \theta) \quad (4)
\end{aligned}$$

or for the case of $\theta_H = 0^\circ$, $\varphi_{M,1} = 0^\circ$ but $\varphi_{M,2} = 90^\circ$ (J_2 dominated), we have

$$\begin{aligned}
2H \sin \theta_{M,1} = & \frac{1}{2} H_{B,1} \sin^2 \theta_{M,1} \sin 2\theta_{M,1} - H_{\text{keff},1} \sin 2\theta_{M,1} \\
& - \frac{2 \sin \theta_{M,1} \cos \theta_{M,2}}{t_1 M_{s,1}}
\end{aligned}$$

$$\begin{aligned}
& \times (J_1 + 2J_2 \cos \theta_{M,1} \cos \theta_{M,2}) \\
2H \sin \theta_{M,2} = & -H_{\text{keff},2} \sin 2\theta_{M,2} - \frac{2 \sin \theta_{M,2} \cos \theta_{M,1}}{t_2 M_{s,2}} \\
& \times (J_1 + 2J_2 \cos \theta_{M,1} \cos \theta_{M,2}) \quad (5)
\end{aligned}$$

with $\Delta\varphi = \varphi_{M,1} - \varphi_{M,2}$, $\theta = \theta_{M,1} + \theta_{M,2}$. The effective perpendicular anisotropy field is defined as $H_{\text{keff},i} = H_{K,i} - 4\pi M_{s,i}$, which is about -1.82 ± 0.02 T for $H_{\text{keff},1}$ and -1.50 ± 0.05 T for $H_{\text{keff},2}$. The difference mainly arises from the slightly different saturation magnetizations.

According to Eqs. (3)–(5), the $J_{1(2)}$ values can be numerically deduced by fitting the magnetization curves with an in-plane or out-of-plane external magnetic field, see Fig. 2(c) for the case of $t_{\text{Ru}} = 1.1$ nm. The fitted J_1 and J_2 from the in-plane curves are illustrated in Fig. 2(d), both of which show a second peak at $t_{\text{Ru}} \sim 1.2$ nm. Such a variation trend was also reported in the Fe/Cr/Fe system [44], which was interpreted as the intrinsic biquadratic coupling mechanism with a loose-spin model [45–47]. Meanwhile, from Eqs. (3)–(5), we can recognize that in the saturated state the equivalent coupling constant J_{eff} can be described as $J_{\text{eff}} = J_1 + 2J_2$. The calculated effective coupling constant J_{eff} values are summarized in Fig. 2(e) as a function of t_{Ru} . Apparently, the results obtained by fitting the in-plane and out-of-plane magnetization curves are identical, showing the same variation trend with t_{Ru} . Subsequently, we substitute J_1 and J_2 into Eq. (3) to calculate the theoretical remanence ratio of η . As expected, without considering J_2 , the calculated remanence ratio remains 0.71 until $t_{\text{Ru}} = 2.0$ nm, above which the IEC disappears, see the blue dashed line in Fig. 2(b). After taking J_2 into consideration, η exhibits two distinctive peaks, verifying that the nonmonotonic behavior of η arises from the strong biquadratic coupling term. Quantitatively, we define the bilinear coupling field as $H_{\text{ex},1} = (J_1/2)[(1/M_{s,1}t_1) + (1/M_{s,2}t_2)]$ and the biquadratic coupling field as $H_{\text{ex},2} = J_2[(1/M_{s,1}t_1) + (1/M_{s,2}t_2)]$ [48]. When $|H_{\text{ex},2}|$ is larger than $|H_{\text{ex},1}|$, i.e., $2|J_2| > |J_1|$, a large η is induced because in this case M_1 and M_2 are canted with an angle of $\phi = -\cos(H_{\text{ex},1}/H_{\text{ex},2})$ without

considering the biaxial anisotropy field. As expected, the experimental peak positions of η just fall in the region of $2|J_2| > |J_1|$, coinciding well with the theoretically calculated ones. Note that some expected deviations between the experimental and theoretical η values in Fig. 2(b) arise mainly from the single domain approximation used in the Stoner-Wolfarth coherent rotation model. We treat each layer as a single domain and calculate the theoretical values without considering the nucleation process influence from unavoidable defects and imperfections. Nevertheless, the main features of the two peaks are clearly described by this simple model.

B. Dynamic magnetic measurements by TRMOKE

As we know, for a SAF system, the magnetizations of the two FM layers will precess together coherently or in an out-of-phase mode. The dynamic IEC always coexists with the static coupling, making it difficult to differentiate their effects on the magnetization dynamics and clarify the profound relations between the static and dynamic parts. To solve this issue, in earlier studies a sufficiently thick NM layer was usually employed to suppress the static IEC

[27,49]. Nevertheless, it has been demonstrated that the static IEC can also be effectively modulated by varying the pump-laser fluences [23,42,50], thus independent magnetization precession or switching of the two FM layers can be realized. So, in this study, instead of increasing the interlayer thickness, the dynamic IEC studies are performed under various pump fluences. It is found that the biaxial anisotropy makes little difference on the magnetization dynamics in this study, so the following results are presented only for the case of $\varphi_H = 0^\circ$.

Figure 3(a) shows the TRMOKE curves measured at different pump-laser fluences for the trilayer sample with $t_{\text{Ru}} = 1.7$ nm and $H = 12.3$ kOe. For the sample pumped at low fluences, we observe one coherent precession mode resulting from the coupled FM₁ and FM₂. As the laser fluence rises, multiple precession modes can be clearly identified; the collective mode is gradually divided into two relatively independent modes [23]. A typical fast Fourier transform (FFT) power spectrum is shown in the inset of Fig. 3(a). Obviously, in addition to the main resonance peak (f_1) with a higher frequency, there exists an additional peak with a relatively lower frequency (f_2). In order to accurately determine the precession frequency and

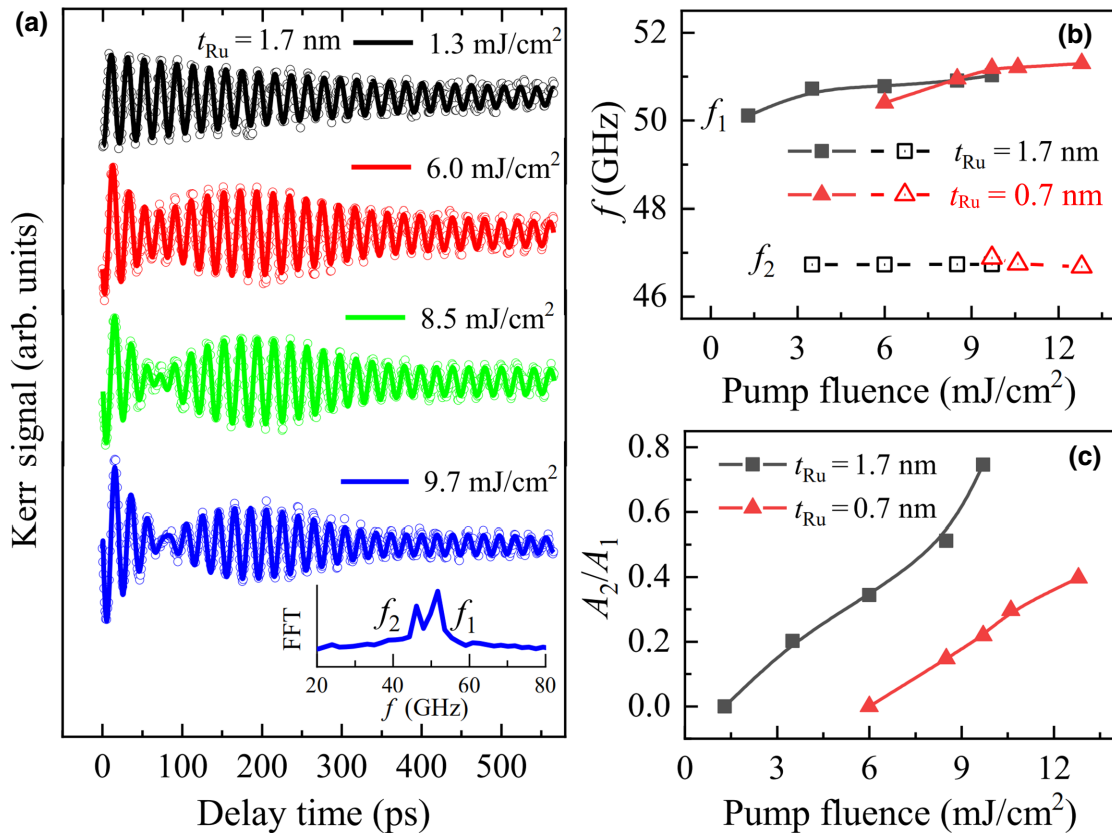


FIG. 3. (a) Laser-induced transient TRMOKE signals (open circles) and the fitting curves (solid lines) measured under various pump fluences but the same applied field of 12.3 kOe for a trilayer sample with $t_{\text{Ru}} = 1.7$ nm. The inset is the FFT of frequency spectrum at the pump fluence of 9.7 mJ/cm². (b) and (c) The pump fluence dependences of the precession frequencies of f_2 and f_1 , as well as their amplitude ratio of A_2/A_1 for two representative samples with $t_{\text{Ru}} = 1.7$ nm and 0.7 nm, respectively.

amplitude, the oscillatory TRMOKE curves in Fig. 3(a) are fitted by the sum of two harmonic damping functions [51],

$$\Delta\theta_k = \sum_{i=1}^2 A_i \exp(-t/\tau_i) \sin(2\pi f_i t + \varphi_i), \quad (6)$$

where the parameters of A_i , τ_i , f_i , and φ_i ($i = 1, 2$) are the precession amplitude, lifetime, frequency, and initial phase of the two modes. The pump-laser fluence dependences of precession frequencies are shown in Fig. 3(b) for the samples of $t_{\text{Ru}} = 0.7$ and 1.7 nm. Owing to the reduced IEC induced by laser heating, the f_1 value that arises from the coherent precession shows a slight increase with increasing pump fluence, which tends to saturate as the static IEC vanishes. By comparing with the precession frequencies for the single Co-Fe(5 nm) and Co-Fe(10 nm) films, we recognize that f_1 is dominated by the thick FM₁ layer while f_2 is related to the thin FM₂ layer. The amplitude ratio of A_2/A_1 is summarized in Fig. 3(c). As expected, the A_2/A_1 ratio increases gradually with the pump fluences, demonstrating that the precession component of FM₂ increases with decreasing IEC strength. Moreover, we can find that

the critical pump fluence required to realize separate magnetization precessions increases with the IEC strength. For instance, noticeable precession of the f_2 mode emerges at 3.5 mJ/cm² for $t_{\text{Ru}} = 1.7$ nm while it significantly increases up to 9.7 mJ/cm² for $t_{\text{Ru}} = 0.7$ nm with much stronger AFM coupling. In the subsequent studies, a fixed pump-laser fluence as high as 9.7 mJ/cm² is chosen to decouple the trilayers with $t_{\text{Ru}} \geq 0.5$ nm. Under this pump condition, the static IEC is severely suppressed and the dynamic IEC in the asymmetric structure begins to play a dominant role in the magnetic damping.

Figure 4(a) shows the representative TRMOKE signals as a function of t_{Ru} under $H = 12.3$ kOe. It can be seen that, except for the directly coupled sample without a Ru spacer, two precession modes can be distinguished upon laser excitation with a fluence of 9.7 mJ/cm². All the measured TRMOKE curves are fitted with Eq. (6), and the obtained precession frequencies and lifetimes are displayed in Figs. 4(b) and 4(c) as a function of the external field H . As previously discussed for Fig. 3, the high frequency precession f_1 is dominated by the thick FM₁ layer while the low frequency f_2 is related to the thin FM₂ layer.

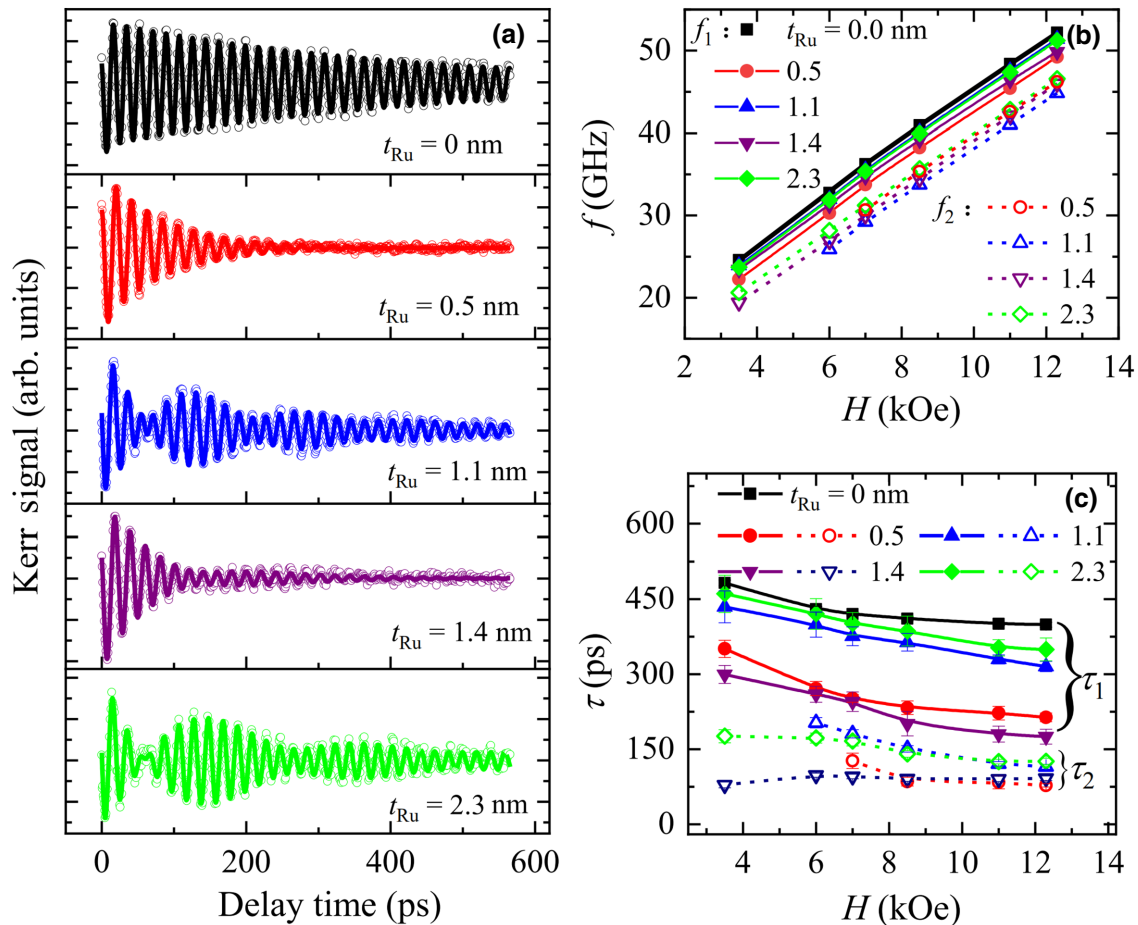


FIG. 4. (a) Laser-induced transient TRMOKE signals (open circles) and the corresponding fitting curves (solid lines) measured at $H = 12.3$ kOe for the samples with various t_{Ru} . (b) and (c) The external field dependences of the precession frequencies and lifetimes.

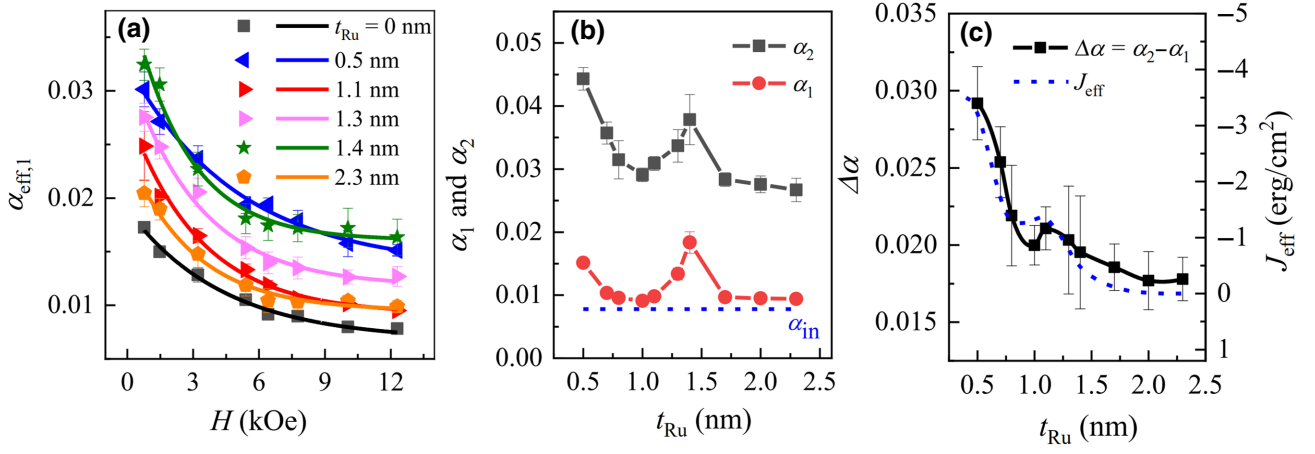


FIG. 5. (a) The calculated effective magnetic damping factor $\alpha_{\text{eff},1}$ versus H with various t_{Ru} . (b) The saturated magnetic damping factor of α_1 and α_2 as a function of t_{Ru} ; the blue dashed line denotes the intrinsic damping of single Co-Fe layer. (c) The t_{Ru} dependences of damping factor difference $\Delta\alpha$ and static IEC strength J_{eff} .

Apparently, the precession frequency f and lifetime τ are greatly dependent on the Ru layer thickness, showing a strong nonmonotonic variation trend with increasing t_{Ru} . In order to deeply understand the effects of the static and dynamic IEC, we further calculate the effective magnetic damping factor by utilizing the formula $\alpha_{\text{eff}} = 1/(2\pi f\tau)$ [52]. Figure 5(a) displays the curves of $\alpha_{\text{eff},1}$ versus H for the FM₁ layer only, which first decreases with increasing H and eventually remains nearly unchanged when H is higher than 12 kOe, because the extrinsic damping contributions from magnetic inhomogeneities get severely suppressed.

For the convenience of analysis, we define the saturated damping factors of FM₁₍₂₎ as $\alpha_{1(2)}$, which are shown in Fig. 5(b) as a function of t_{Ru} . As compared to α_1 , the α_2 value is much larger than the intrinsic damping of 0.008 for the single Co-Fe layer. This is understandable since the spin pumping damping contribution is inversely proportional to the FM layer thickness [53]. Remarkably, both curves exhibit a nonmonotonic behavior, showing a maximum value at $t_{\text{Ru}} = 1.4$ nm. According to the t_{Ru} dependence of J_{eff} , we would expect an IEC-related spin pumping damping peak occurring at $t_{\text{Ru}} \sim 1.2$ nm. The observed damping peak shift may arise from the overlap of this peak with an additional peak located at a slightly larger Ru thickness. The extra peak can be generated from the superposition of the conventional spin pumping damping and an abnormal damping contribution with opposite dependences on the Ru interlayer thickness [54]. For $t_{\text{Ru}} < \lambda_{\text{SD}}/2$, it has been reported that with t_{Ru} increasing, the former increases due to the increased absorption of spin current within the Ru layer, while the latter decreases as the spin back current reduces. Nevertheless, according to our experiments and the published results of other researchers [55,56], the Co-Fe layer capped with Ru cannot generate such a big enhancement in damping due

to its weak spin-orbit coupling interaction. There may still exist some other extrinsic causes responsible for the observed peak at around 1.4 nm. To address this issue, we define the obtained magnetic damping factor α_i ($i = 1$ or 2) as

$$\alpha_i = \alpha_{\text{in},i} + \alpha_{\text{SP},i} + \alpha_{\text{ex},i}. \quad (7)$$

$\alpha_{\text{in},i}$ is the intrinsic damping of the FM _{i} layer, which can be taken as a constant. $\alpha_{\text{ex},i}$ describes the extrinsic damping contributions from magnetic inhomogeneities and two-magnon scattering, which can be efficiently suppressed by the large applied external field of 12.3 kOe. To remove the disturbance of other factors and highlight the spin pumping damping $\alpha_{\text{SP},i}$, we define the damping difference as $\Delta\alpha = \alpha_2 - \alpha_1$. According to the above analysis, $\Delta\alpha$ should be proportional to $\Delta\alpha_{\text{SP}}$, mostly arising from the dynamic IEC between the two FM layers. As depicted in Fig. 5(c), for our AFM coupled asymmetric trilayers, $\Delta\alpha_{\text{SP}}$ exhibits a quite similar variation tendency to the calculated J_{eff} , suggesting that the additional spin pumping damping arising from the dynamic IEC is mainly determined by the strength of static IEC. The damping factor peaks of α_2 and α_1 at $t_{\text{Ru}} = 1.4$ nm are shifted towards $t_{\text{Ru}} = 1.2$ nm for $\Delta\alpha$, since most of the extrinsic contributions and partial spin pumping damping have been canceled out. Based on these results, we propose a modified approximate expression of spin pumping damping that applies to the AFM coupled trilayer system [30],

$$\Delta\alpha_{\text{SP}} = \frac{g\mu_B}{4\pi} \left(\frac{g_{\text{eff},2}^{\uparrow\downarrow}}{M_{s,2}t_2} - \frac{g_{\text{eff},1}^{\uparrow\downarrow}}{M_{s,1}t_1} \right) \beta J_{\text{eff}}, \quad (8)$$

where μ_B is Bohr magneton, $g_{\text{eff},1(2)}^{\uparrow\downarrow}$ are the effective interfacial spin mixing conductances of FM_{1(2)}/Ru, and β is}

a coefficient. Equation (8) demonstrates that the stronger the AFM coupling is, the larger the spin pumping damping will be.

IV. CONCLUSION

In conclusion, we perform a comprehensive investigation of the static and dynamic magnetic properties in $\text{Co}_{80}\text{Fe}_{20}/\text{Ru}/\text{Co}_{80}\text{Fe}_{20}$ asymmetric trilayers. The remanence ratio η of hard axis ($\varphi_H = 45^\circ$) to easy axis ($\varphi_H = 0^\circ$) is found to be nonmonotonic with t_{Ru} due to the large biquadratic coupling J_2 . The TRMOKE measurements indicate two individual precessions are stimulated by increasing the pump-laser fluence due to the reduction of the static IEC strength. The damping factor α is found to exhibit an obvious maximum value at $t_{\text{Ru}} = 1.4$ nm, which is attributed to the key role of dynamic IEC via the mutual spin currents induced in the asymmetric trilayers. Furthermore, the difference of spin pumping damping $\Delta\alpha_{\text{SP}}$ is found to show a similar t_{Ru} dependence to that of J_{eff} , revealing a close relation between the dynamic and static IEC. Our results provide insights into the effect of dynamic IEC on the magnetization dynamics in exchange-coupled SAF structures, which contribute to the engineering of microwave spintronic devices with tunable magnetic damping and oscillation frequency.

ACKNOWLEDGEMENTS

This work is supported by the National Natural Science Foundation of China (Grants No. 52171230, No. 11874120, No. 12074072, and No. 51671057).

-
- [1] M. N. Baibich, J. M. Broto, A. Fert, F. N. Van Dau, F. Petroff, P. Etienne, G. Creuzet, A. Friederich, and J. Chazelas, Giant Magnetoresistance of (001)Fe/(001)Cr Magnetic Auperlattices, *Phys. Rev. Lett.* **61**, 2472 (1988).
 - [2] P. Grünberg, R. Schreiber, Y. Pang, M. B. Brodsky, and H. Sowers, Layered Magnetic Structures: Evidence for Antiferromagnetic Coupling of Fe Layers Across Cr Interlayers, *Phys. Rev. Lett.* **57**, 2442 (1986).
 - [3] P. A. Grünberg, Exchange anisotropy, interlayer exchange coupling and GMR in research and application, *Sens. Actuator A Phys.* **91**, 153 (2001).
 - [4] B. N. Engel, J. Akerman, B. Butcher, R. W. Dave, M. DeHerrera, M. Durlam, G. Grynkeiwich, J. Janesky, S. V. Pietambaram, N. D. Rizzo, J. M. Slaughter, K. Smith, J. J. Sun, and S. Tehrani, A 4-Mb toggle MRAM based on a novel bit and switching method, *IEEE Trans. Magn.* **41**, 132 (2005).
 - [5] E. E. Fullerton, D. T. Margulies, M. E. Schabes, M. Carey, B. Gurney, A. Moser, M. Best, G. Zeltzer, K. Rubin, H. Rosen, and M. Doerner, Antiferromagnetically coupled magnetic media layers for thermally stable high-density recording, *Appl. Phys. Lett.* **77**, 3806 (2000).
 - [6] A. Lyle, S. Patil, J. Harms, B. Glass, X. Yao, D. Lilja, and J. Wang, Magnetic tunnel junction logic architecture for realization of simultaneous computation and communication, *IEEE Trans. Magn.* **47**, 2970 (2011).
 - [7] R. A. Duine, K.-J. Lee, S. S. P. Parkin, and M. D. Stiles, Synthetic antiferromagnetic spintronics, *Nat. Phys.* **14**, 217 (2018).
 - [8] M. Wang, W. Cai, K. Cao, J. Zhou, J. Wrona, S. Peng, H. Yang, J. Wei, W. Kang, Y. Zhang, J. Langer, B. Ocker, A. Fert, and W. Zhao, Current-induced magnetization switching in atom-thick tungsten engineered perpendicular magnetic tunnel junctions with large tunnel magnetoresistance, *Nat. Commun.* **9**, 671 (2018).
 - [9] S.-H. Yang, K.-S. Ryu, and S. Parkin, Domain-wall velocities of up to 750 m s^{-1} driven by exchange-coupling torque in synthetic antiferromagnets, *Nat. Nanotechnol.* **10**, 221 (2015).
 - [10] M. Xu, D. Meng, J. Zhang, R. Li, G. Jiang, and Z. Zhang, Suppression of the repulsion phenomenon of magnetic skyrmions at the end of synthetic antiferromagnetic racetracks, *J. Phys. Condens. Matter* **33**, 495801 (2021).
 - [11] R. Lavrijsen, J.-H. Lee, A. Fernández-Pacheco, D. C. M. C. Petit, R. Mansell, and R. P. Cowburn, Magnetic ratchet for three-dimensional spintronic memory and logic, *Nature* **493**, 647 (2013).
 - [12] Y.-C. Lau, D. Betto, K. Rode, J. M. D. Coey, and P. Stamenov, Spin-orbit torque switching without an external field using interlayer exchange coupling, *Nat. Nanotechnol.* **11**, 758 (2016).
 - [13] S. Łazarski, W. Skowroński, J. Kanak, Ł. Karwacki, S. Ziętek, K. Grochot, T. Stobiecki, and F. Stobiecki, Field-Free Spin-Orbit-Torque Switching in Co/Pt/Co Multilayer with Mixed Magnetic Anisotropies, *Phys. Rev. Appl.* **12**, 014006 (2019).
 - [14] Y. Sheng, K. W. Edmonds, X. Ma, H. Zheng, and K. Wang, Adjustable current-induced magnetization switching utilizing interlayer exchange coupling, *Adv. Electron. Mater.* **4**, 1800224 (2018).
 - [15] H. J. Waring, N. A. B. Johansson, I. J. Vera-Marun, and T. Thomson, Zero-Field Optic Mode Beyond 20 GHz in a Synthetic Antiferromagnet, *Phys. Rev. Appl.* **13**, 034035 (2020).
 - [16] S. Li, Q. Li, J. Xu, S. Yan, G.-X. Miao, S. Kang, Y. Dai, J. Jiao, and Y. Lü, Tunable optical mode ferromagnetic resonance in FeCoB/Ru/FeCoB synthetic antiferromagnetic trilayers under uniaxial magnetic anisotropy, *Adv. Funct. Mater.* **26**, 3738 (2016).
 - [17] S. Zhang, J. Lin, G.-X. Miao, S. Li, G. Zhao, X. Wang, Q. Li, D. Cao, J. Xu, S. Yan, and Y. Lü, Ultrahigh frequency and anti-interference optical-mode resonance with biquadratic coupled FeCoB/Ru/FeCoB trilayers, *ACS Appl. Mater. Interfaces* **11**, 48230 (2019).
 - [18] S. Li, C. Wang, X.-M. Chu, G.-X. Miao, Q. Xue, W. Zou, M. Liu, J. Xu, Q. Li, Y. Dai, S. Yan, S. Kang, Y. Long, and Y. Lü, Engineering optical mode ferromagnetic resonance in FeCoB films with ultrathin Ru insertion, *Sci. Rep.* **6**, 33349 (2016).
 - [19] N. X. Sun and G. Srinivasan, Voltage control of magnetism in multiferroic heterostructures and devices, *SPIN* **02**, 1240004 (2012).

- [20] Z. Chen and V. G. Harris, Ferrite film growth on semiconductor substrates towards microwave and millimeter wave integrated circuits, *J. Appl. Phys.* **112**, 081101 (2012).
- [21] T. Kuribara, M. Yamaguchi, and K. Arai, Equivalent circuit analysis of an RF integrated ferromagnetic inductor, *IEEE Trans. Magn.* **38**, 3159 (2002).
- [22] G. Wu, S. Chen, Y. Ren, Q. Y. Jin, and Z. Zhang, Laser-induced magnetization dynamics in interlayer-coupled $[\text{Ni}/\text{Co}]_4/\text{Ru}/[\text{Co}/\text{Ni}]_3$ perpendicular magnetic films for information storage, *ACS Appl. Nano Mater.* **2**, 5140 (2019).
- [23] J. Zhou, S. Saha, Z. Luo, E. Kirk, V. Scagnoli, and L. J. Heyderman, Ultrafast laser induced precessional dynamics in antiferromagnetically coupled ferromagnetic thin films, *Phys. Rev. B* **101**, 214434 (2020).
- [24] C. He, G. Yu, C. Grezes, J. Feng, Z. Zhao, S. A. Razavi, Q. Shao, A. Navabi, X. Li, Q. L. He, M. Li, J. Zhang, K. L. Wong, D. Wei, G. Zhang, X. Han, P. K. Amiri, and K. L. Wang, Spin-Torque Ferromagnetic Resonance in W/Co-Fe-B/W/Co-Fe-B/MgO Stacks, *Phys. Rev. Appl.* **10**, 034067 (2018).
- [25] P. Bruno and C. Chappert, Oscillatory Coupling Between Ferromagnetic Layers Separated by a Nonmagnetic Metal Spacer, *Phys. Rev. Lett.* **67**, 1602 (1991).
- [26] Y. Pogoryelov, M. Pereiro, S. Jana, A. Kumar, S. Akansel, M. Ranjbar, D. Thonig, D. Primetzhofer, P. Svedlindh, J. Åkerman, O. Eriksson, O. Karis, and D. A. Arena, Non-reciprocal spin pumping damping in asymmetric magnetic trilayers, *Phys. Rev. B* **101**, 054401 (2020).
- [27] B. Heinrich, Y. Tserkovnyak, G. Woltersdorf, A. Brataas, R. Urban, and G. E. W. Bauer, Dynamic Exchange Coupling in Magnetic Bilayers, *Phys. Rev. Lett.* **90**, 187601 (2003).
- [28] Y. Li, Y. Li, R. Sun, N. Li, Z.-Z. Gong, X. Yang, Z.-K. Xie, H.-L. Liu, W. He, X.-Q. Zhang, and Z.-H. Cheng, Anomalous Gilbert damping induced by the coexisting static and dynamic coupling in Fe/Pd/Fe trilayers, *Phys. Rev. B* **104**, 094409 (2021).
- [29] Z. Zhu, B. Zhao, W. Zhu, M. Tang, Y. Ren, Q. Y. Jin, and Z. Zhang, Annealing effect and interlayer modulation on magnetic damping of CoFeB/interlayer/Pt thin films, *Appl. Phys. Lett.* **113**, 222403 (2018).
- [30] S. Azzawi, A. Ganguly, M. Tokaç, R. M. Rowan-Robinson, J. Sinha, A. T. Hindmarch, A. Barman, and D. Atkinson, Evolution of damping in ferromagnetic/nonmagnetic thin film bilayers as a function of nonmagnetic layer thickness, *Phys. Rev. B* **93**, 054402 (2016).
- [31] A. Layadi and J. O. Artman, Ferromagnetic resonance in a coupled two-layer system, *J. Magn. Magn. Mater.* **92**, 143 (1990).
- [32] H. Yang, Y. Li, and W. E. Bailey, Large spin pumping effect in antisymmetric precession of $\text{Ni}_{79}\text{Fe}_{21}/\text{Ru}/\text{Ni}_{79}\text{Fe}_{21}$, *Appl. Phys. Lett.* **108**, 242404 (2016).
- [33] S. Takahashi, Giant enhancement of spin pumping in the out-of-phase precession mode, *Appl. Phys. Lett.* **104**, 052407 (2014).
- [34] K. Lenz, T. Toliński, J. Lindner, E. Kosubek, and K. Baberschke, Evidence of spin-pumping effect in the ferromagnetic resonance of coupled trilayers, *Phys. Rev. B* **69**, 144422 (2004).
- [35] M. Belmeguenai, T. Martin, G. Woltersdorf, M. Maier, and G. Bayreuther, Frequency- and time-domain investigation of the dynamic properties of interlayer-exchange-coupled $\text{Ni}_{81}\text{Fe}_{19}/\text{Ru}/\text{Ni}_{81}\text{Fe}_{19}$ thin films, *Phys. Rev. B* **76**, 104414 (2007).
- [36] A. Ghosh, S. Auffret, U. Ebels, and W. E. Bailey, Penetration Depth of Transverse Spin Current in Ultrathin Ferromagnets, *Phys. Rev. Lett.* **109**, 127202 (2012).
- [37] D. Wu, Z. Zhe, L. Le, Z. Zhang, H. B. Zhao, J. Wang, B. Ma, and Q. Y. Jin, Perpendicular magnetic anisotropy and magnetization dynamics in oxidized CoFeAl films, *Sci. Rep.* **5**, 12352 (2015).
- [38] A. Azevedo, C. Chesman, S. M. Rezende, F. M. de Aguiar, X. Bian, and S. S. P. Parkin, Biquadratic Exchange Coupling in Sputtered (100) Fe/Cr/Fe, *Phys. Rev. Lett.* **76**, 4837 (1996).
- [39] G. J. Strijkers, J. T. Kohlhepp, H. J. M. Swagten, and W. J. M. de Jonge, Origin of Biquadratic Exchange in Fe/Si/Fe, *Phys. Rev. Lett.* **84**, 1812 (2000).
- [40] S. O. Demokritov, Biquadratic interlayer coupling in layered magnetic systems, *J. Phys. D* **31**, 925 (1998).
- [41] Y. Shiota, T. Taniguchi, M. Ishibashi, T. Moriyama, and T. Ono, Tunable Magnon-Magnon Coupling Mediated by Dynamic Dipolar Interaction in Synthetic Antiferromagnets, *Phys. Rev. Lett.* **125**, 017203 (2020).
- [42] B. Khodadadi, J. B. Mohammadi, J. M. Jones, A. Srivastava, C. Mewes, T. Mewes, and C. Kaiser, Interlayer Exchange Coupling in Asymmetric Co-Fe/Ru/Co-Fe Trilayers Investigated with Broadband Temperature-Dependent Ferromagnetic Resonance, *Phys. Rev. Appl.* **8**, 014024 (2017).
- [43] E. C. Stoner and E. P. Wohlfarth, A mechanism of magnetic hysteresis in heterogeneous alloys, *Phil. Trans. R. Soc. A* **240**, 599 (1948).
- [44] A. J. R. Ives, J. A. C. Bland, R. J. Hicken, and C. Daboo, Oscillatory biquadratic coupling in Fe/Cr/Fe(001), *Phys. Rev. B* **55**, 12428 (1997).
- [45] D. M. Edwards, J. M. Ward, and J. Mathon, Intrinsic and secondary mechanisms for biquadratic exchange coupling in magnetic trilayers, *J. Magn. Magn. Mater.* **126**, 380 (1993).
- [46] U. Köbler, K. Wagner, R. Wiechers, A. Fuß, and W. Zinn, Higher order interaction terms in coupled Fe/Cr/Fe sandwich structures, *J. Magn. Magn. Mater.* **103**, 236 (1992).
- [47] R. P. Erickson, K. B. Hathaway, and J. R. Cullen, Mechanism for non-Heisenberg-exchange coupling between ferromagnetic layers, *Phys. Rev. B* **47**, 2626 (1993).
- [48] G. Wu, W. Zhu, Z. Zhu, H. Xue, Y. Ren, Y. Liu, Q. Y. Jin, and Z. Zhang, Magnetic precession modes with enhanced frequency and intensity in hard/NM/soft perpendicular magnetic films, *Phys. Chem. Chem. Phys.* **21**, 16830 (2019).
- [49] B. Heinrich, G. Woltersdorf, R. Urban, and E. Simanek, Role of dynamic exchange coupling in magnetic relaxations of metallic multilayer films (invited), *J. Appl. Phys.* **93**, 7545 (2003).
- [50] Z. Zhang, L. Zhou, P. E. Wigen, and K. Ounadjela, Using Ferromagnetic Resonance as a Sensitive Method to Study Temperature Dependence of Interlayer Exchange Coupling, *Phys. Rev. Lett.* **73**, 336 (1994).

- [51] Y. Zhang, G. Wu, W. Zhu, Z. Ji, Q. Y. Jin, and Z. Zhang, Controllable magnetization precession dynamics and damping anisotropy in Co_2FeAl heusler-alloy films, *Phys. Chem. Chem. Phys.* **23**, 12612 (2021).
- [52] G. Malinowski, K. C. Kuiper, R. Lavrijsen, H. J. M. Swagten, and B. Koopmans, Magnetization dynamics and gilbert damping in ultrathin $\text{Co}_{48}\text{Fe}_{32}\text{B}_{20}$ films with out-of-plane anisotropy, *Appl. Phys. Lett.* **94**, 102501 (2009).
- [53] J. M. Shaw, H. T. Nembach, and T. J. Silva, Determination of spin pumping as a source of linewidth in sputtered $\text{Co}_{90}\text{Fe}_{10}/\text{Pd}$ multilayers by use of broadband ferromagnetic resonance spectroscopy, *Phys. Rev. B* **85**, 054412 (2012).
- [54] X. Yang, S. Zhang, Q. Li, G. Zhao, and S. Li, The abnormal damping behavior due to the combination between spin pumping and spin back flow in $\text{Ni}_{80}\text{Fe}_{20}/\text{Ru}_t$ bilayers, *J. Magn. Magn. Mater.* **502**, 166495 (2020).
- [55] N. Behera, M. S. Singh, S. Chaudhary, D. K. Pandya, and P. K. Muduli, Effect of Ru thickness on spin pumping in Ru/Py bilayer, *J. Appl. Phys.* **117**, 17A714 (2015).
- [56] L. Jin, H. Zhang, X. Tang, F. Bai, and Z. Zhong, Effects of ruthenium seed layer on the microstructure and spin dynamics of thin permalloy films, *J. Appl. Phys.* **113**, 053902 (2013).